Ketonization of Valeric Acid to 5-Nonanone over Metal Oxides catalysts

Ali Alizadeh Eslami, François Devred, Damien P. Debecker*

Université catholique de Louvain (UCLouvain), Institute of Condensed Matter and Nanosciences (IMCN), Louvain-La-Neuve, Belgium

*Corresponding author, email: damien.debecker@uclouvain.be

Abstract

Valeric acid (VA), readily obtainable in the biorefinery from sugary biomass streams, can be upgraded to 5-nonanone, a versatile chemical building block with numerous applications. This study investigates the performance of nine metal oxide catalysts (SnO_2, SiO_2, Y_2O_3, CeO_2, ZrO_2, TiO_2, La_2O_3, Cr_2O_3, and Al_2O_3) in the gas-phase ketonization of VA to 5-nonanone in the 350-450°C range. The screening reveals a correlation between the metal oxides lattice energy and their catalytic activity for valeric acid ketonization. ZrO_2, TiO_2, and La_2O_3, characterized by high lattice energy, demonstrate the highest catalytic activity. Y_2O_3, SnO_2, SiO_2, showing low lattice energy, are barely active. However, exceptions to this trend were observed: Cr_2O_3 and Al_2O_3 displayed poor catalytic performance despite their elevated lattice energy. The comprehensive characterization of the catalysts, encompassing XRD, N_2-physisorption, NH_3-TPD, and CO_2-TPD analyses, has unveiled the crucial role of important parameters including acid-base properties in addition to lattice energy. Only oxides showing amphoteric properties can catalyse the reaction effectively. Interestingly, low-lattice energy and amphoteric oxides such as SnO_2 (showing poor performance) become significantly active at higher temperature (500°C). Analysis of by-products by online GC-MS and spent catalyst characterization indicated that in this case the ketonization mechanism changed from the so-called surface mechanism to the so-called bulk mechanism.

Keywords: Ketonization, Valeric acid, 5-nonanone, Metal oxide catalysts, lattice energy, biofuel, biorefinery

Introduction

The world is grappling with a significant challenge: an impending energy crisis exacerbated by rising energy demands and the depleting availability of fossil fuels. The combustion of fossil fuels is a leading contributor to greenhouse gas emissions, such as carbon dioxide (CO_2), accelerating the degradation of the environment. According to the International Energy Agency, global energy demand is projected to surge by over 20% by 2040. Concurrently, CO_2 emissions from the energy sector could escalate to nearly 40 Gt by 2040, from an estimated 33 Gt in 2021 [1]. In light of these challenges, there's a pressing need to pivot towards alternative and renewable energy sources. Bio-based energy streams present a promising avenue in this endeavor. Life-cycle analyses have highlighted that biofuels can potentially reduce emissions by 40% to 86% when compared to their petroleum counterparts [2].

Lignocellulosic feedstock as the most abundant class of non-edible biomass, and is a potential candidate for both green energy and value-added chemicals production [3]. Indeed, a persistent challenge in biofuel production revolves around the critical need to improve both energy efficiency and sustainability. Many bio-based platform chemicals have a high oxygen content, leading to low calorific values. Moreover, the presence of impurities, such as water, aliphatic OH groups, and carboxylic acids, can complicate further processing and utilization [4-6]. These characteristics often result in fuels with lower energy density, higher viscosity, and corrosive properties, limiting their direct application in standard internal combustion engines [7]. Among the derivatives from biomass, carboxylic acids stand out as a relevant target. For example, valeric acid, which can be produced through the conversion of levulinic acid, serves as a precursor to a variety of essential chemicals [8]. VA and its esters have diverse applications as plasticizers and in pharmaceuticals, cosmetics, and as food additives [9]. Additionally, exploring the production of fuel additives and biofuels from VA presents an intriguing avenue. 5-nonanone, also known as dibutyl ketone (DBK), is an important VA derivative which has

been primarily used as an industrial solvent or as a paint, resin, and fuel additive. The latter application can be attributed to 5-nonanone's higher energy content (as compared to VA) [10]. Additionally, its lower viscosity of 0.96 mm^2/s is advantageous, helping to overcome operational difficulties, while its significantly low melting point of -53°C makes it an ideal seasonal fuel additive [11]. 5-nonanone can be further processed into a C_9 alkene stream via hydrogenation and dehydration. This alkene stream can then be oligomerized to yield C_{18}-C_{27} olefins in high yields. These bio-based olefins, given their optimal molecular weight range, are suitable for jet and diesel fuels. Hence, they may play a pivotal role in fostering a cleaner energy landscape and reducing greenhouse gas emissions [12, 13].

The transformation of VA to 5-nonanone is achieved through ketonization, a process that couples two carboxylic acids into a longer-chain ketone by eliminating water and carbon dioxide (Eq. 1). The process of ketonization was first identified by Friedel in 1858 [14]. This reaction is an effective way to decrease both the oxygen content and the acidity, concurrently forming C-C bonds to produce stable ketone products [15].

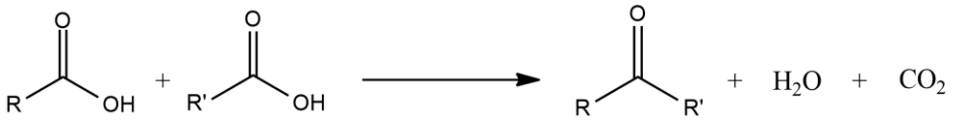

(Eq.1)

The journey to develop efficient catalysts for ketonization has seen significant advancements over the recent years. Despite considerable progress, the understanding of crucial parameters, reaction mechanisms, and active sites in the ketonization of carboxylic acids remains a subject of ongoing discussion. Many investigations have emphasized individual metal oxide catalysts or particular carboxylic acids, leading to a fragmented view that can generate contradictions due to differing setups, feeds, or reaction conditions. Offering a more streamlined perspective, Glinski *e al.*[16] investigated the ketonization of propanoic acid

over 32 metal oxides supported on conventional catalyst supports such as Al_2O_3, SiO_2, and TiO_2. Their research highlighted manganese, zirconium, cerium, thorium, and uranium oxides as particularly effective catalysts. Yet, the key catalyst properties that govern catalyst performance were not identified. Yamada *e al.*[17] investigated the ketonization of acetic acid using 14 rare earth oxides that were calcined at 1000°C. Rare earth oxides such as La_2O_3, CeO_2, Pr_6O_{11}, and Nd_2O_3 achieved relatively high acetic acid conversions, selectively to acetone. However, the scarcity and cost of some rare earth metals might limit their commercial viability. In another study conducted by Almutairi *e al.*[18], the ketonization of acetic acid was explored on γ-Al_2O_3, TiO_2, ZrO_2 and CeO_2 catalysts. CeO_2 emerged as the most effective catalyst, while γ-Al_2O_3 was the least active. The research emphasized the significance of weak basic sites in ketonization, while acidity was claimed to have no impact on activity. This conclusion contrasts with Ding et al.'s findings on $Ce_xZr_{1-x}O_2$ catalysts for propionic acid ketonization [19]. They identified a relationship between the medium-strength acid/base site ratio and the ketonization rate, suggesting the need for an optimal acid–base balance.

To our knowledge, only three studies have been reported specifically on the ketonization of valeric acid (VA). Kulyk *e al.*[20] studied the catalytic pyrolysis of valeric acid on various nanoscale oxides: SiO_2, γ-Al_2O_3, CeO_2/SiO_2, Al_2O_3/SiO_2 and TiO_2/SiO_2. 5-nonanone and propylketene were identified as the main products, and CeO_2/SiO_2 showed the highest selectivity for ketonization. Panchenko *e al.*[21] explored the adsorption of VA and 5-nonanone on zirconia using DRIFTS and UV–vis DRS. Their study pinpointed Lewis acid sites as key for converting valeric acid to 5-nonanone on ZrO_2. In a separate investigation [22], they reported that 10 wt% CeO_2/ZrO_2 demonstrated enhanced catalytic activity, compared to pure zirconia. Their findings also suggested that a hydrogen atmosphere, as opposed to nitrogen, resulted in higher valeric acid conversion.

Considering the above, it appears evident that bond strength between metal and oxygen [23], and acid-base sites [24] play a crucial role in the ketonization reaction. To better understand the ketonization of VA and enhance its efficiency, a deeper dive into the processes and mechanisms is indispensable. Two reaction pathways have been proposed in the ketonization reaction: surface and bulk mechanisms [24]. Lattice energy has been introduced as an important factor affecting the reaction mechanism. The strength of the metal-oxygen bond is reflected in the lattice energy; it is a measure of the energy required to separate the constituent ions of a solid into gaseous ions. In the context of metal oxides, a higher lattice energy suggests stronger metal-oxygen bonds, which can influence the catalyst's stability and reactivity. The lattice energy can be estimated using the Born-Haber cycle, which is based on Hess's law. This cycle considers the various enthalpy changes involved in the formation of an ionic compound, including ionization energy, electron affinity, sublimation enthalpy, bond dissociation enthalpy, and the lattice energy [25, 26].

The surface mechanism involves the direct reaction of carboxylic acids on the surface of the catalysts. The surface mechanism typically occurs over metal oxides with high lattice energies (*e.g.*, MnO_2, TiO_2, ZrO_2, CeO_2, SnO_2, etc.). Various theories regarding surface mechanisms have been suggested, encompassing ketene based, concerted, anhydride, and a β-ketoacid mechanisms [27, 28]. In contrast, the bulk mechanism is favored on metal oxides with either low lattice energy or high basicity. Initially the carboxylic acids undergo deprotonation on the metal oxides and forms metal carboxylate salts (MCS) and lattice hydroxyls. Upon heating to a sufficiently high temperature, the MCS undergo thermal decomposition to produce bulk metal carbonate and a ketone as the desired product. Then, the metal carbonate may react with the hydroxyl group to be regenerated to the original metal oxide and release CO_2 and H_2O [29-31].

This study investigates the ketonization of VA over a series of metal oxide catalysts (SnO_2, SiO_2, Y_2O_3, CeO_2, ZrO_2, TiO_2, La_2O_3, Cr_2O_3, Al_2O_3) to understand how catalyst properties – particularly metal oxygen bond strength and nature of acid-base sites – influence reaction efficiency. By screening metal oxides showing different lattice energy, under same reaction conditions, we highlight the importance of this parameter. General trends in catalytic behavior and performance are further established by investigating catalysts acido-basicity and reducibility, by inspecting the nature of the reaction by-products, and by characterizing the spent catalysts. From the point of view of catalyst performance evaluation, our approach differs from the previously reported studies on VA ketonization, in two key aspects. First, online GC-MS provides accurate and time-resolved analysis of catalytic performance (unlike the generally adopted method of analyzing the products collected in a cold trap over the time of the reaction). Second, we use a relatively high liquid hourly space velocity and VA concentration, allowing to target high specific productivity for 5-nonanone.

1 Materials and Methods

1.1 Catalyst Preparation

To synthesize the metal oxides, the following precursors were used: $ZrO(NO_3)_2 \cdot xH_2O$ (99%, Sigma Aldrich), TiO_2 (99.9%, Degussa P25), γ-Al_2O_3 (99.97%, 3 Micron APS powder, Alfa Aesar), Cr_2O_3 (99%, Acros), $Ce(NO_3)_3 \cdot 6H_2O$ (99%, Sigma Aldrich), $Y(NO_3)_3 \cdot 6H_2O$ (99.8%, Sigma Aldrich), $La(NO_3)_3 \cdot 6H_2O$ (99%, Sigma Aldrich), SiO_2 (Silica gel 60, Merck), $SnCl_4$ (98%, Sigma Aldrich). The precursor salts were calcined to obtain the corresponding metal oxide. The calcination was performed in air at 500°C for 4h. The heating rate was 5°C/min. Commercial γ-Al_2O_3, and Cr_2O_3 powders were also calcined in the same conditions.

1.2 Catalyst Characterization

The textural properties were evaluated through nitrogen (N_2) adsorption-desorption isotherms at -196°C, using the Tristar 3000 apparatus (Micromeritics, USA). Prior to measurement, the samples were degassed at 150°C over night under vacuum. The surface area was determined using the Brunauer-Emmett-Teller (BET) method in the relative pressure range of 0.05 to 0.30.

X-ray diffraction (XRD) analyses were carried out on a Bruker-D8 advance diffractometer with a Bragg-Brentano geometry, using a LynxEye XE-T detector with Cu $K\alpha_{1,2}$ radiation (λ=0.154178 nm, 40 kV, 30 mA). The diffractograms were taken in a 2θ range between 5° and 80° (2.2°/min). HighScore Plus software (Ver. 5.1) was used to execute phase identification [32]. The crystallite size was calculated using the Scherrer equation wherein it was applied to the most intense diffraction peak of each oxide.

NH_3 and CO_2 temperature-programmed desorption (TPD) experiments were performed using the CATLAB-PCS (Hiden Analytical) instrument equipped with a mass spectrometer. The samples were initially degassed at 250°C for 1.5 hours under an argon flow of 30 mL/min. Subsequently, adsorption was performed at 60°C for 1 hour using either a 5% NH_3 in He mixture (10 mL/min) supplemented with 20 mL/min of argon, or a 15% CO_2 in argon mixture (30 mL/min), followed by argon purging. Desorption was then carried out by heating the samples to 750°C at a rate of 10°C/min under an argon flow of 30 mL/min.

A dedicated VA-TPD experiment was also carried out after contacting the catalyst with liquid VA, to identify the desorption products. 200 mg of catalyst powder was impregnated with 0.1 mL VA. Then it was dried at 120 °C for 5 hours to remove excess VA. The BELCAT II instrument (Microtrac®), equipped with a mass spectrometer, was used for effluent detection. The analysis was conducted under a continuous argon flow of 30 mL/min. Initially, the sample

was held at 120 °C for 1 hour, followed by a temperature ramp to 710 °C at a rate of 10 °C/min. Throughout the analysis, mass spectrometry monitored the desorption or production of surface species. Mass-to-charge (m/z) ratios of 18, 44, 57, and 60 were chosen to represent H_2O, CO_2, 5-nonanone, and VA, respectively.

1.3 Experimental Setup for Catalytic Performance Test

The catalytic activity was evaluated using a fixed-bed tandem µ-Reactor (Rx-3050TR system from Interscience) loaded with 50 mg of catalyst. The catalyst was pelletized and sieved to a size range of 40-50 mesh. It was fixed in the middle of the µ-reactor, between two layers of quartz beads and wool, in a "sandwich"-like reactor configuration. A feed stream of Valeric acid (99%, Sigma Aldrich) was injected with a high-precision syringe pump (Chemyx Fusion 100), and diluted in a countercurrent flow with 60 ml/min flow of He to achieve a final concentration of approximately 5.5 mol%. The quantitative analysis of the reaction gaseous mixture species was performed using GC/MS (TRACE 1300/ISQ-MS 7000 thermo-scientific) equipped with a Restek stabilwax capillary column (30 m × 0.32 mm × 1 µm). Collected data was processed by Chromeleon 7.3 software.VA conversion, selectivity, and yields are defined according equations (2), (3), and (4).

$$Conversion(\%) = \frac{C_V^0 - C_V}{C_V^0} \times 100 \qquad \text{(Eq.2)}$$

$$Selectivity(\%) = \frac{2 \times C_{5N}}{C_V^0 - C_V} \times 100 \qquad \text{(Eq.3)}$$

$$Yield\ (\%) = \frac{2 \times C_{5N}}{C_V^0} \times 100 \qquad \text{(Eq.4)}$$

Where C_V is the concentration of unreacted VA, C_V^0 is the concentration of inlet fed valeric (~5%), and C_{5N} is the concentration of the produced ketone (molar%). The factor of 2 in the selectivity formula accounts for the stoichiometry of the ketonization reaction.

2 Results and discussions

2.1 Catalytic activity in the ketonization of valeric acid

A series of metal oxides with different metal-oxygen bond strength (indicated by the lattice energy) was studied. Figure 1 shows the catalytic performance of all synthesized metal oxide catalysts in the ketonization of VA at 350, 400, and 450°C. ZrO_2 demonstrated the highest conversion and yield followed by TiO_2, La_2O_3, CeO_2, and Y_2O_3. Conversely, Cr_2O_3 was totally inactive, SnO_2 and SiO_2 exhibited poor catalytic activity under all reaction conditions, and Al_2O_3 showed moderately activity only at 450°C but still much lower than other active catalysts.

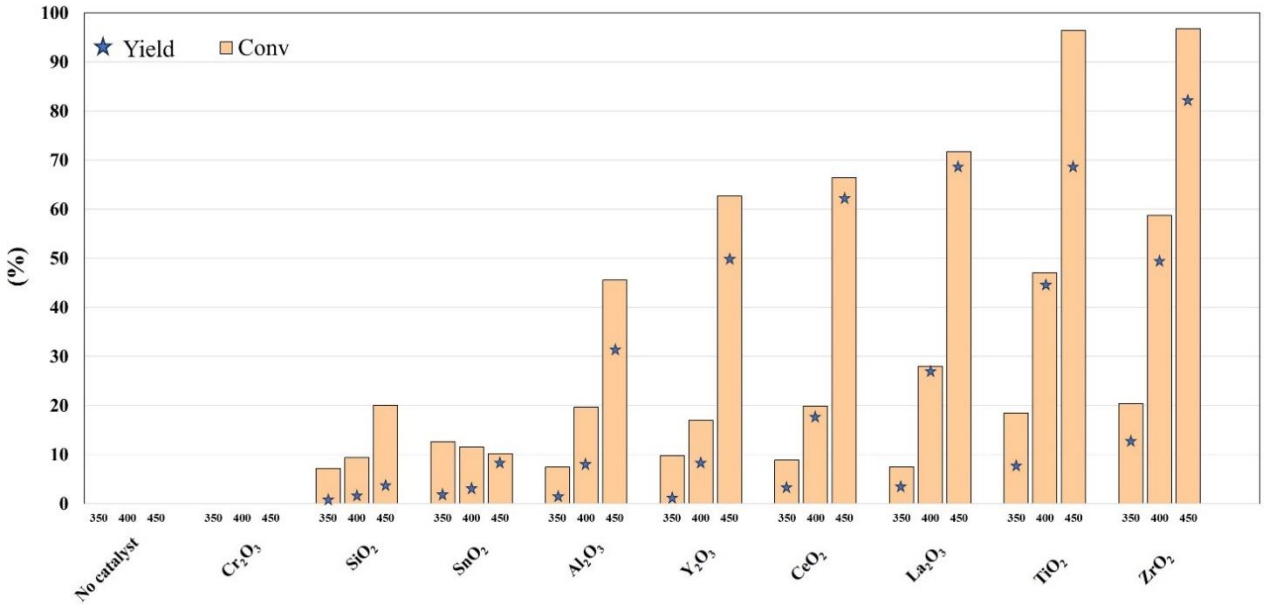

Figure 1. Catalytic performance (conversion and yield) in the ketonization of VA over metal oxide catalysts.

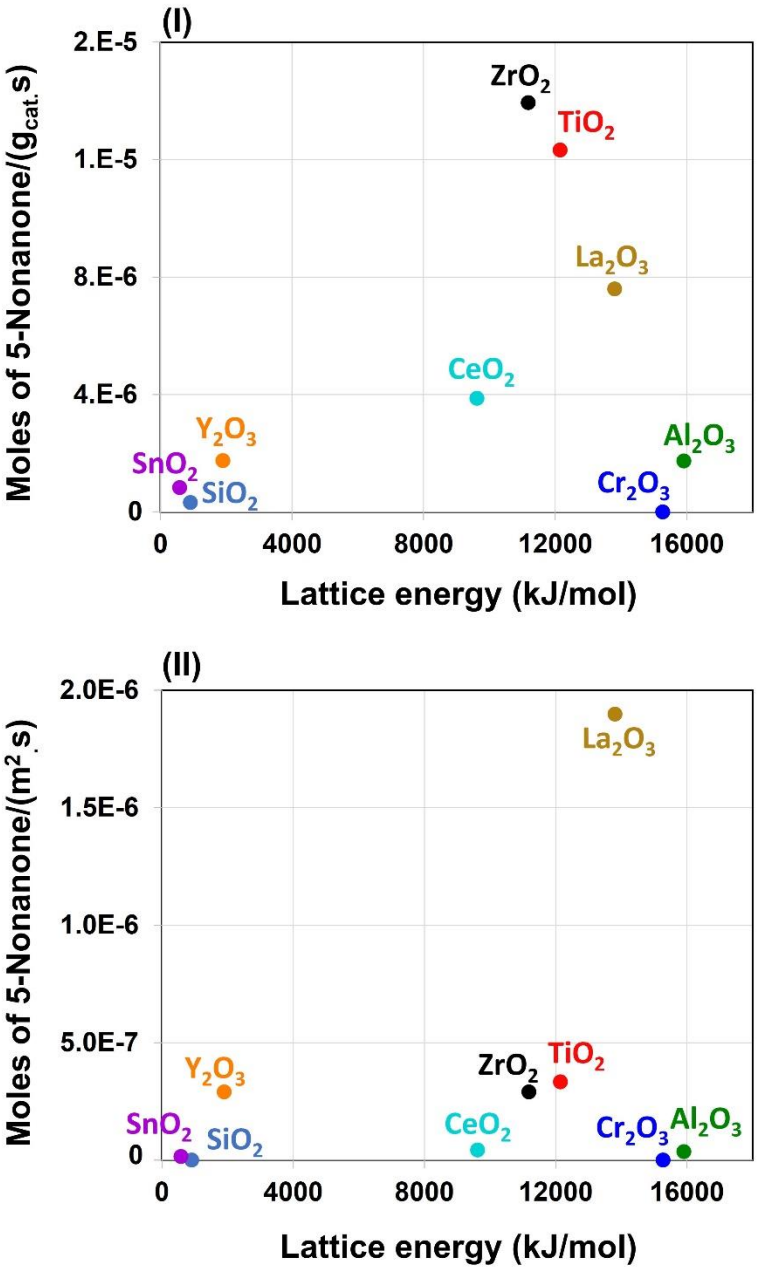

Figure 1. 5-Nonanone productivity at 400 °C vs. metal oxide lattice energy normalized based on (I) mass and (II) specific surface area of the catalyst.

Figure 2(I) shows the catalytic performance (expressed in terms of 5-nonanone productivity at 400°C) as a function of the lattice energy of the oxide. Oxides with high lattice energy (Zr, T, and to some extent Ce and La oxides) showed high activity. On the contrary, Y, Si and Sn oxides have very low lattice energy and showed very low ketonization activity.

The catalytic activity of metal oxides in ketonization reactions has been linked to their lattice energy, which influences the prevailing reaction mechanism (either bulk or surface). Notably, CeO_2 [31] and La_2O_3 [17] have been observed to switch between these mechanisms depending on the reaction temperature.

Our findings revealed exceptions: Cr_2O_3 and Al_2O_3, despite possessing high lattice energy, displayed minimal ketonization yield. This observation suggests that other catalyst properties play a crucial role alongside lattice energy. We will further explore this concept in the light of acid-base characterization, which can significantly impact catalytic activity.

Furthermore, Figure 2 (II) presents the molar flow of 5-nonanone normalized by the catalyst's specific surface area, plotted against the lattice energy of various metal oxides. While the overall trend from Figure 3.2 (I) remains largely consistent, normalizing by specific surface area reveals some intriguing deviations. Notably, La_2O_3 exhibits an exceptionally high value, suggesting significant intrinsic activity when accounting for the available reaction surface.

2.2 Catalyst characterization

2.2.1 Texture and structure

The N_2-physisorption results (Table 1) show that SiO_2 has the highest specific surface area (SSA) at 350 m^2/g, followed by CeO_2 at 89 m^2/g, TiO_2 at 37 m^2/g, and ZrO_2 at 48 m^2/g. In contrast, La_2O_3 and Cr_2O_3 have the lowest specific surface area at 4 and 2 m^2/g, respectively. Note that while Cr_2O_3 was inactive, La_2O_3 exhibited significantly higher catalytic activity despite its very low SSA.

Table 1. Textural properties of the synthesized catalysts.

Catalyst	Lattice energy (kJ/mol) [23]	S_{BET} (m^2/g)	Pore vol. (cm^3/g)*	Cryst. size (nm)**	Crystal system
Al_2O_3	15916	47	0.22	12	Cubic
Cr_2O_3	15276	2	0.013	120	Hexagonal

La_2O_3	13814	4	0.05	23	Cubic, Hexagonal
TiO_2	12150	37	0.13	37	Tetragonal***
ZrO_2	11188	48	0.18	14	Tetragonal Monoclinic
CeO_2	9627	89	0.23	10	Cubic
Y_2O_3	1905	6	0.005	10	Cubic
SiO_2	911	359	0.8	-	-
SnO_2	588	51	0.38	6	Tetragonal

* Pore volume determined using the BJH method.
** Determined using the Scherrer equation.
***Tetragonal TiO_2 exists as two polymorphs: Anatase and Rutile.

The XRD patterns of the synthesized metal oxide catalysts are shown in Figure 3. For ɣ-Al_2O_3, the cubic phase was identified through characteristic peaks at 2θ = 19, 32, 37, 39, 46, 61, and 67 ° (JCPDS: # 96-120-0016) [33]. The hexagonal phase of Cr_2O_3 was characterized at 2θ = 24, 34, 36, 39, 41, 44, 50, 54, 63, 65, 73, 76, and 79° (JCPDS: # 96-900-8085) [34].

The cubic phase of La_2O_3 was marked by distinct peaks at angles 2θ of 27, 31, 40, 44, and 53° (JCPDS: # 96-153-7843) [35]. Additionally, minor indications of the hexagonal phase for La_2O_3 were noticed at 2θ = 30° and 46° (JCPDS: # 96-410-2406) [36].

TiO_2 catalyst showed the coexistence of anatase and rutile phases. About 86% of the composition was found to be the anatase phase, with characteristic peaks detected at 2θ values of 25, 37, 47, 55, and 62° (JCPDS: # 96-900-9087). The rutile phase was recognized with peaks at 2θ values of 27, 36, 41, and 56° (JCPDS: # 96-900-9084) [37].

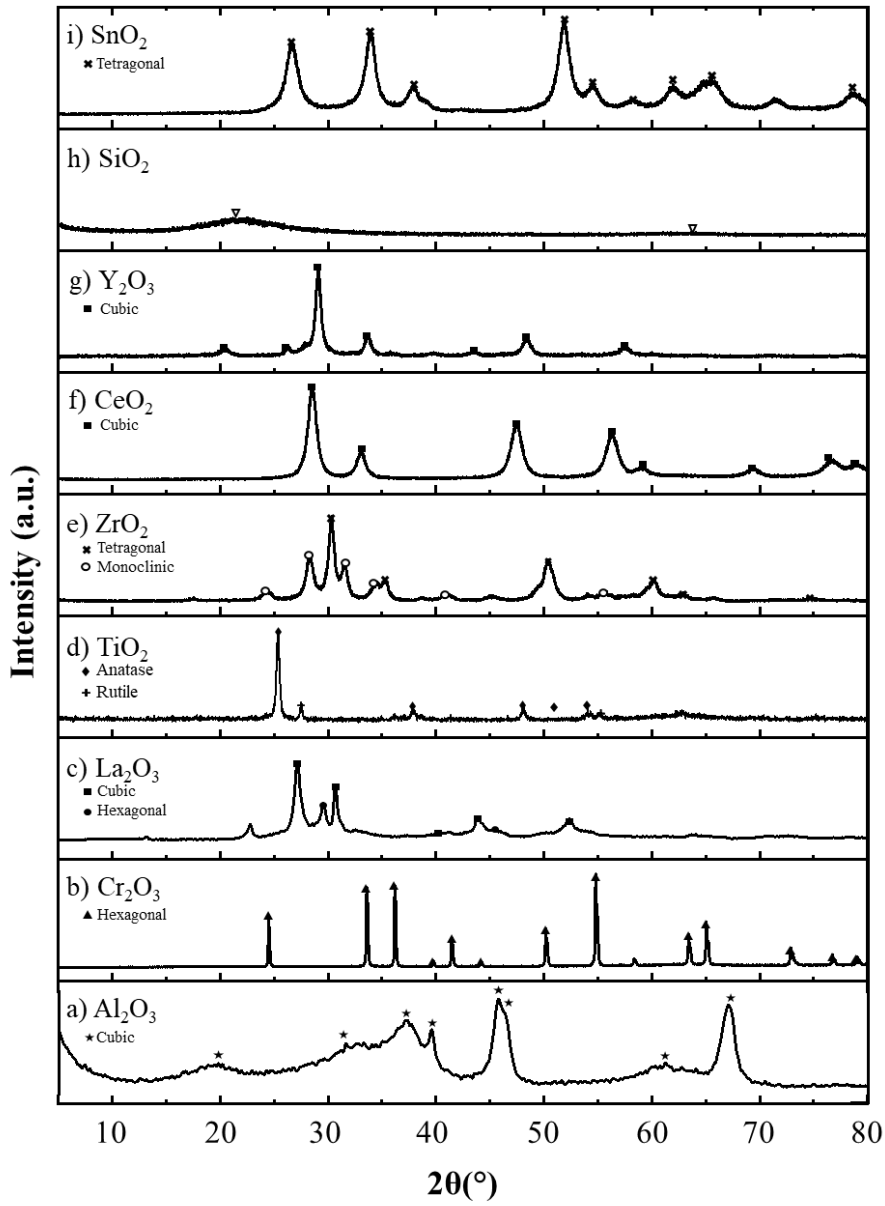

Figure 3. XRD Patterns of the Synthesized catalysts.

It is known that ZrO_2 can exist in three crystalline polymorphs: monoclinic, tetragonal, and cubic [38]. Here, ZrO_2 showed the coexistence of both tetragonal and monoclinic phases. The tetragonal phase was identified by the characteristic peaks at 2θ values of 30, 35, 51, 60, 63, and 74° (JCPDS: # 96-230-0613), and the monoclinic phase was detected with diffraction lines at 2θ values of 24, 28, 31, 34, 42, and 56° (JCPDS: # 96-900-5834) [39]. CeO_2 had a cubic phase, as evidenced by characteristic peaks observed at 2θ = 28, 33, 47, 56, 59, 69, 76, and 78° (JCPDS: # 96-900-9009) [37]. The cubic phase of Y_2O_3 was found with peaks at 2θ values of 26,

29, 34, 40, 43, 48, and 57° (JCPDS: # 96-101-0588) [40]. SiO_2 catalyst was amorphous, exhibiting only the broad signal at about 22° (JCPDS: # 96-900-8235) [41]. The tetragonal phase of SnO_2 was indicated by the peaks at 2θ values of 26, 34, 38, 52, 54, 57, 62, 66, and 78° (JCPDS: # 96-153-4786) [42].

Different crystal facets of a metal oxides expose distinct active sites with varying coordination and electronic properties, potentially impacting reactant adsorption and reaction pathways. It has been suggested that the specific adsorption mode of the carboxylic acid on the catalyst surface can significantly influence the ketonization reaction. Different adsorption configurations, including monodentate and bidentate (bridging and chelating) modes, are possible. Monodentate adsorption, where the carboxylate molecule occupies only one active site, can provide a higher number of available active sites compared to bidentate adsorption, potentially leading to enhanced catalytic activity [19, 21].

2.2.2 Acido-basicity

Figures 4 and 5 show the NH_3-TPD and CO_2-TPD results of the synthesized catalysts. Table 2 provides a comprehensive overview of the total acidity and basicity in µmol/g and µmol/m^2. The acid/base site ratio reflects the relative abundance of total acidic and basic sites, categorizing the catalysts into three groups: amphoteric, predominantly acidic, and predominantly basic.

ZrO_2 and CeO_2 exhibit a balanced acid-base character with acid/base site ratios close to 1. Al_2O_3 shows a higher concentration of acidic sites compared to basic sites, as reflected in their acid/base site ratios greater than 1. La_2O_3 and Y_2O_3 display a higher concentration of basic sites than acidic sites, indicated by their acid/base site ratios less than 1. Cr_2O_3, with its notably low concentration of both acidic and basic sites, can be considered neutral. While SSA plays a role, the intrinsic nature of the metal oxide and its surface chemistry also significantly

influences the concentration and strength of acid-base sites. For example, La_2O_3, despite its low SSA, exhibits a high density of basic sites (10 μmol/m²), surpassing other catalysts with higher SSA.

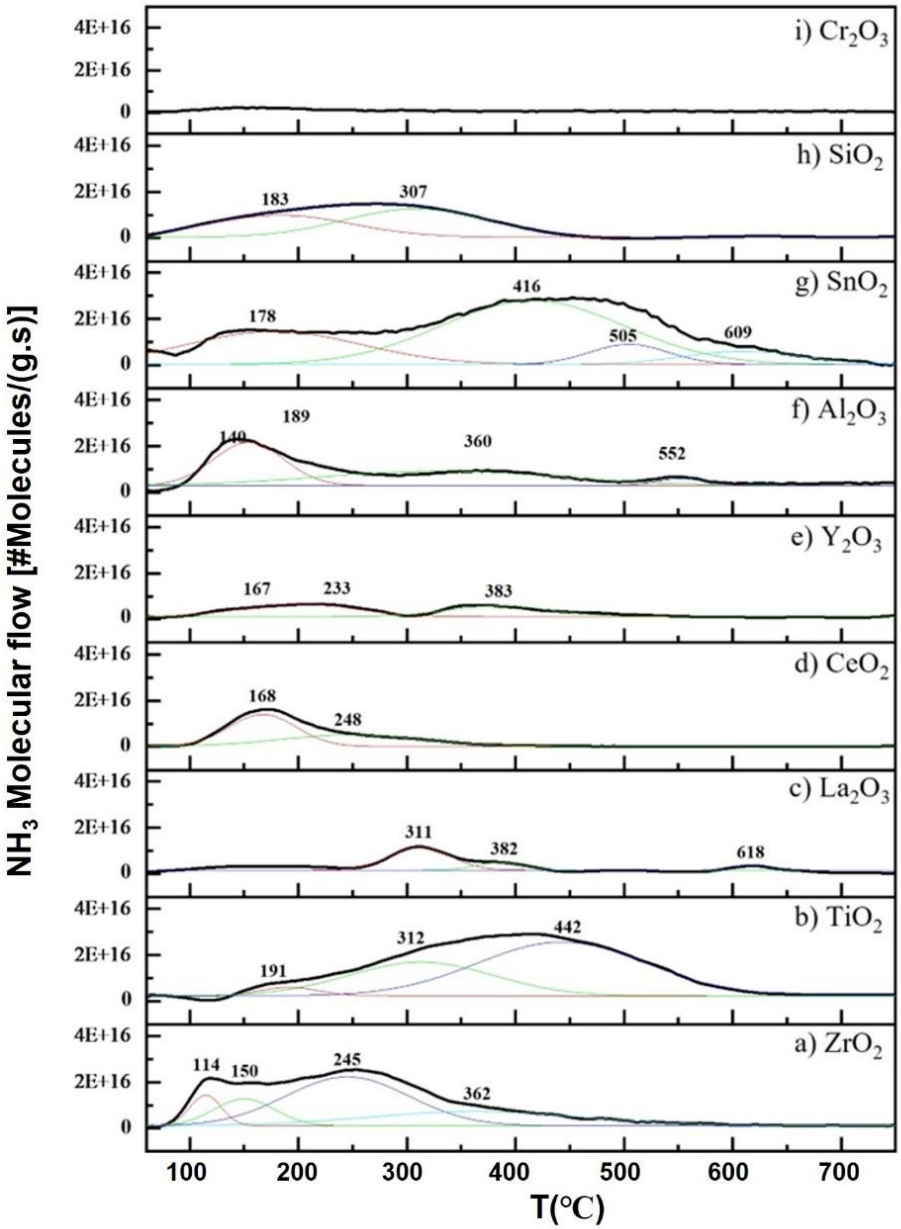

Figure 4. NH_3-TPD results of the synthesized catalysts.

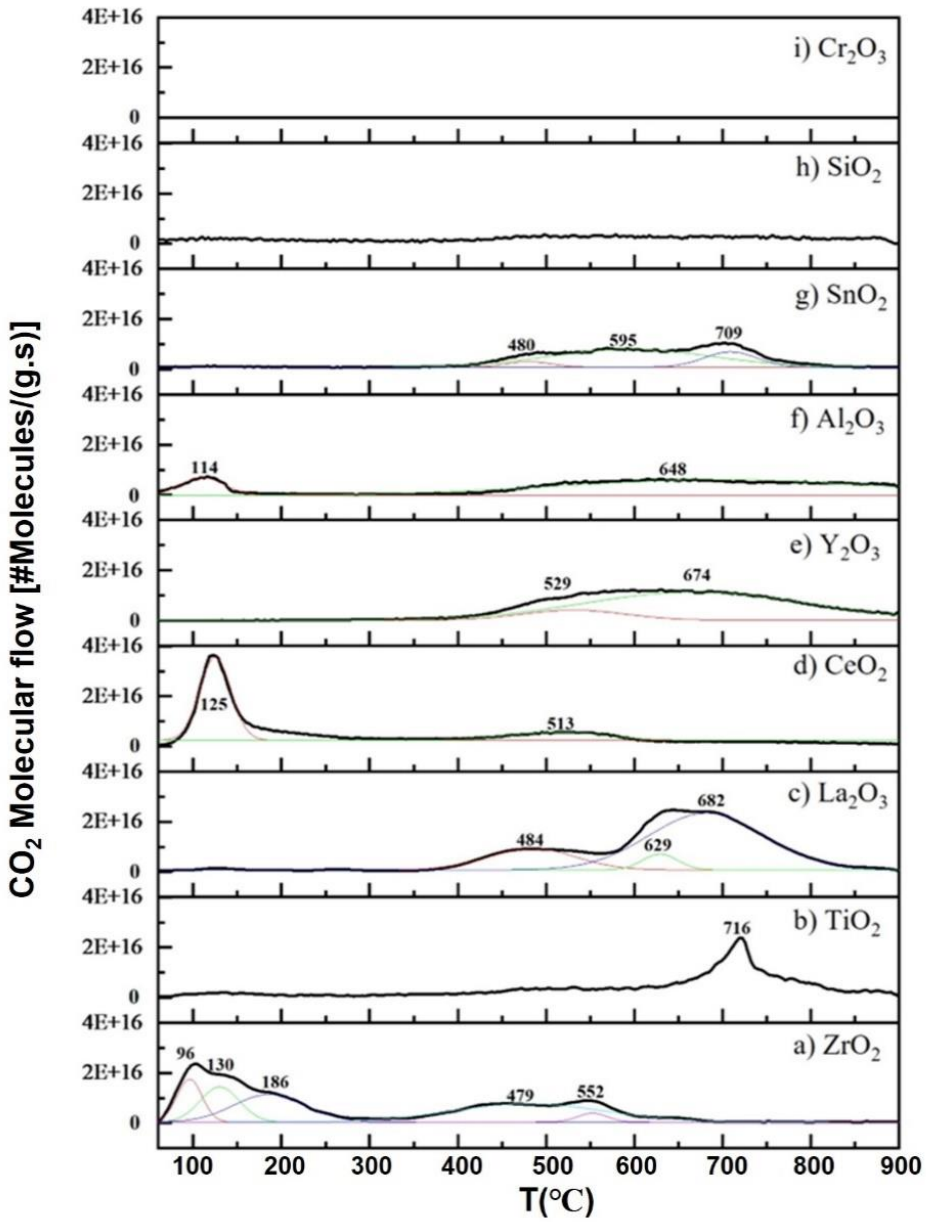

Figure 5. CO_2-TPD results of the synthesized catalysts.

A correlation likely exists between acid to base ratio and catalytic activity in VA ketonization. ZrO_2, which exhibits the highest catalytic activity, possesses a balanced acid-base character. Yazdanpanah *et al.* [43] studied the catalytic performance of TiO_x catalysts in the ketonization of methyl palmitate. They emphasized the importance of having both Lewis acid and Brønsted base sites for effective ketonization. Specifically, Lewis acid sites were found to facilitate ketone production, whereas Brønsted acid sites could lead to unwanted byproducts. The ketone formation rate was closely tied to the density of acid sites, and the selectivity for

the target ketone product depended on the balance between Lewis and Brønsted acid sites. TiO_2, with high catalytic activity showed an imbalanced acid-to-base ratio, which is indeed unexpected. It's important to acknowledge that the quantification of acid and base sites, while informative, provides a simplified picture of the catalyst's surface chemistry. The current analysis relies on total acidity and basicity values, which may not fully capture the complexity of the active sites and their interactions with the reactants. Additionally, we calculated the total acidity and basicity up to 500°C and 300°C (ESI Tables S2 and S3); however, no clear correlation between these acid-base properties and catalyst activity was observed. This indicates that additional factors, such as lattice energy, surface area, and crystal structure, may also significantly influence the catalyst's performance in valeric acid ketonization.

On the other hand, catalysts with predominantly acidic (*e.g.* SnO_2) or basic (*e.g.* La_2O_3, CeO_2, and Y_2O_3) character display lower catalytic activity. Cr_2O_3, with its neutral character, is inactive. A balanced acid-base character appears to be crucial for achieving high catalytic activity. The literature supports this hypothesis. Pulido *et al.* [15] suggested that the initial step of ketonization involves deprotonation of the carboxylic acid through the α hydrogen by a basic site, forming a β-keto acid intermediate. The subsequent step involves decarboxylation of the β-keto acid followed by the protonation by an acidic site to release the ketone. In other words, the presence of both acidic and basic sites in pairs appears to be essential for achieving high catalytic activity in the ketonization reaction [19, 28].

Table 2. Acid-Base properties of synthesized catalysts (Cal.)

Catalyst	Total Acidity (μmol/g)	Total Surface Acidity (μmol/m^2)	Total Basicity (μmol/g)	Total Surface Basicity (μmol/m^2)	Acid/Basic sites[a]
Al_2O_3	40	0.8	25	0.5	1.6
Cr_2O_3	4	2	0.06	0.03	-
La_2O_3	15	3	40	10	0.4
TiO_2	60	1.5	15	0.4	4

ZrO_2	40	0.9	45	1	0.9
CeO_2	13	0.15	31	0.45	0.4
Y_2O_3	15	2.4	40	7	0.4
SiO_2	20	0.07	0.01	0.05	-
SnO_2	70	1.3	30	0.6	2.3

[a] Calculated as ration between Total Acidity (µmol/g) and Total Basicity (µmol/g). No value is reported for Cr and Si oxides, because the extremely low basicity values lead to extremely high values for the ratio, which have little quantitative meaning.

We observed that catalysts with high lattice energy, but imbalanced acid-base properties showed low activity. In this regard, Rawesh *et al.* [44], have reported that light rare earth metal oxides, such as La_2O_3, Pr_6O_{11}, CeO_2, and Nd_2O_3, exhibit strong basicity, enabling them to engage in the bulk mechanism by directly forming metal oxyacetates in the ketonization of acetic acid.

It is suggested that an effective catalyst for VA ketonization must possess a synergistic combination of amphoteric properties and high lattice energy. However, further investigation is needed to achieve a better understanding on the complex interplay between factors determining the catalytic performance. To gain further insight, we propose examining two specific cases of poorly active oxides (SnO_2 and Cr_2O_3) and to compare them with ZrO_2 as the most active catalyst.

2.3 Investigating the factors behind SnO_2's poor catalytic activity versus ZrO_2 in VA Ketonization

To understand the limitations of SnO_2 as a ketonization catalyst, we investigated the effect of increasing reaction temperature. A substantial increase in 5-nonanone yield was observed with increasing temperature (ESI Figure 1). However, even at higher temperatures, the catalytic performance of SnO_2 remained significantly lower than ZrO_2.

While the yield remained low at 1.7% and 2.9% for 350°C and 400°C, respectively, a significant improvement was observed at higher temperatures, with the yield rising from 8.2%

at 450°C to 25.4% at 500°C (ESI, Figure S1). Interestingly, at lower temperatures, despite the conversion of VA, the yield of 5-nonanone was very low (in other words 5-nonanone selectivity is low). This observation aligns with the findings of Yakerson *e al.*[45], who studied the catalytic ketonization of acetic acid. In their work, using MgO, PbO, and Bi_2O_3 as catalysts, a decrease in acid concentration was observed well before the formation of products. This led the authors to propose, for the first time, the existence of a bulk reaction mechanism for ketonization.

As illustrated in Figure 6i, this mechanism begins with the formation of metal carboxylate salts and lattice hydroxyls. A significant increase in ketone yield was observed at higher temperatures.

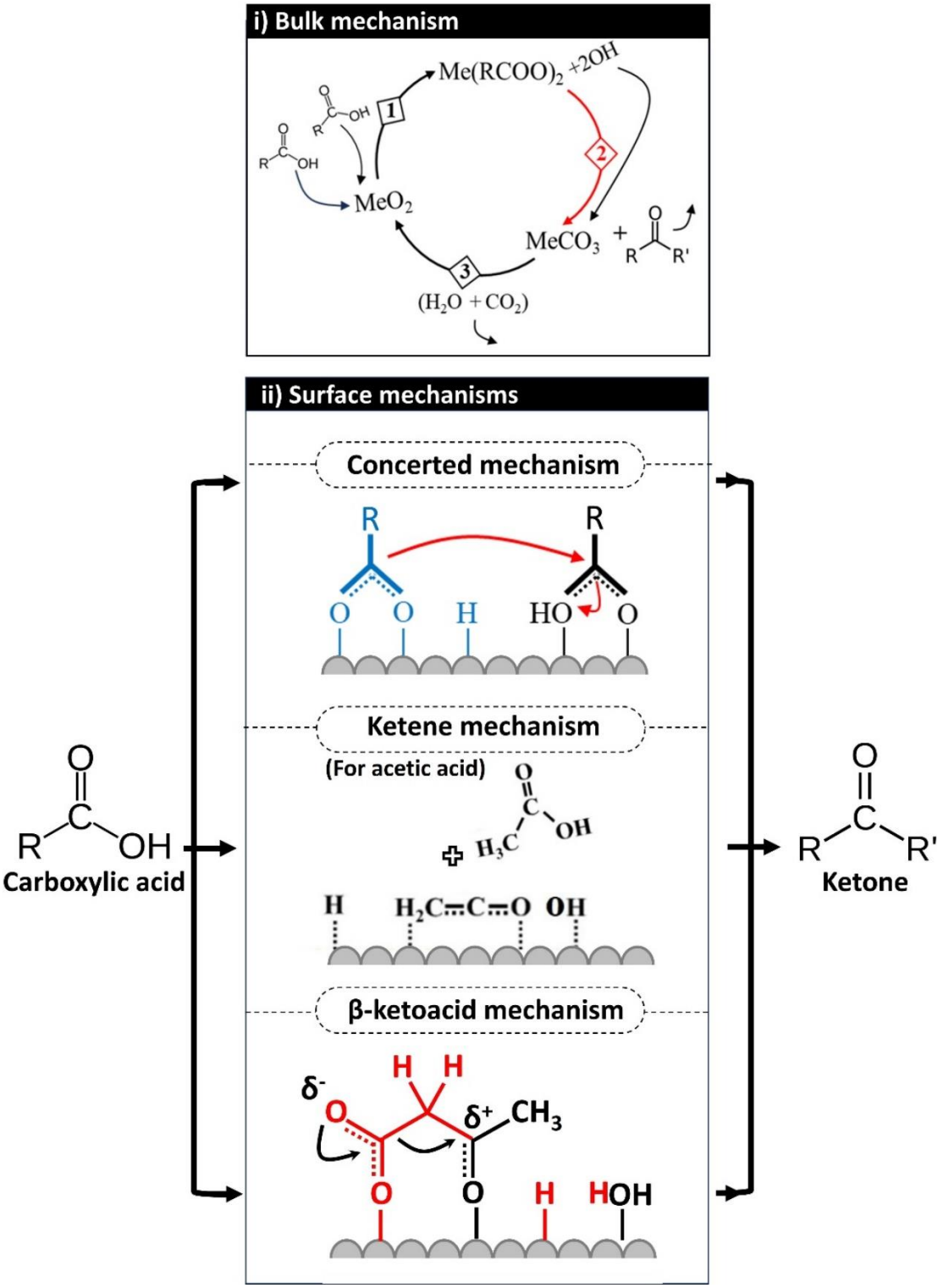

Figure 6. Schematic of i) bulk reaction mechanism, and ii) surface mechanisms in carboxylic acid ketonization

Subsequently, the metal carbonate can react with lattice hydroxyls, regenerating the original metal oxide and releasing CO_2 and H_2O. This observation for SnO_2, that the yield of 5-nonanone increases significantly at higher temperatures, suggests that the bulk mechanism may

play a role in the ketonization of VA over SnO_2, although further investigation is required to confirm this hypothesis.

In contrast, the surface mechanism (ii) occurs directly on the catalyst surface and can proceed through various routes, including the concerted [15], ketene [28], and β-ketoacid [46-48] mechanisms. The concerted mechanism involves simultaneous formation of carbon-carbon bonds and carbon dioxide. The ketene mechanism proceeds via the formation of a ketene intermediate, while the β-ketoacid mechanism involves the formation of a β-ketoacid intermediate. In the surface ketonization mechanisms, the catalyst acts as a stage where the reactants come together and react. The stage itself remains unchanged during the process. It is important to note that the bulk mechanism can jeopardize catalyst with the risk of restructuring, potentially hindering the complete recovery of the original structure [30]. To investigate this possibility, we examined the crystal structures of fresh and spent SnO_2 and ZrO_2 catalysts at low and high reaction temperatures using XRD analysis.

Figure 7 displays the XRD analysis of fresh SnO_2 and ZrO_2 catalysts after reaction at 350°C and 500°C for a short period of 30 min. The XRD patterns for ZrO_2 remained unaffected, indicating the stability of the catalyst across the temperature range tested. On the contrary, a noticeable alteration was observed in the XRD patterns of SnO_2 catalysts used at 500°C, which exhibited additional peaks at 2θ values of 30, 32, 44, 46, 55, 73, and 74° [37]. These correspond to the presence of metallic Sn (JCPDS: # 96-900-8571) [37] and it suggests the occurrence of catalyst restructuring, consistent with the bulk mechanism. The observed reduction of SnO_2 could be due to several factors. At the high temperature it is plausible that the side reactions, leading to the formation of by-products that could act as reducing agents.

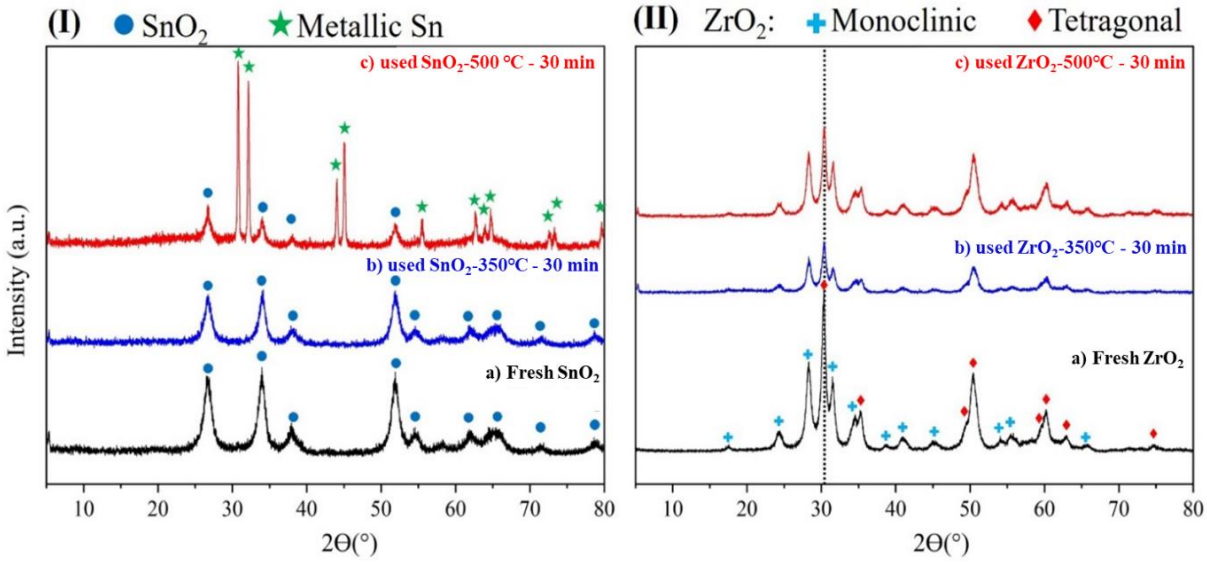

Figure 7. XRD patterns for the fresh and used (I) SnO_2, and (II) ZrO_2 catalysts.

Although SnO_2 reactivity increased at higher temperatures, its overall performance remained significantly lower than ZrO_2. This aligns with previous research suggesting that the bulk mechanism for ketonization is less efficient due to the formation of additional intermediates and lower selectivity towards the desired ketone [24, 44, 49]. To further investigate this, we focused on analyzing the by-products formed during the reaction at low and high temperatures (ESI Table S1). Even though these by-products are present in very small amounts compared to 5-nonanone, they still can provide valuable insights into the reaction pathways. In the VA ketonization over SnO_2, short-chain carboxylic acids, particularly acetic and propanoic acids, were observed as byproducts at lower reaction temperatures (350°C and 400°C). These compounds were not seen with ZrO_2 under similar reaction conditions. This observation could be attributed to the cleavage of the α-carbon-hydrogen bond in VA during the formation of valerate salts on the SnO_2 surface. The low lattice energy of SnO_2 may facilitate this cleavage, leading to the formation of these short-chain acids as by-products. At higher temperatures (450, 500°C), the formation of these short-chain acids diminishes, and 5-nonanone becomes the prominent product, accompanied with other by-products such as ketones (*e.g.*, 2-hexanone),

alkenes (*e.g.*, 3,5-octadiene), and aldehydes (*e.g.*, heptanal and 2-methylheptanal). In contrast, the absence of short-chain acid by-products and the higher selectivity towards 5-nonanone observed with ZrO_2 even at low temperatures, suggest a different dominant reaction pathway. In fact, ZrO_2, with its higher lattice energy, primarily follows a surface mechanism.

To study the behavior of chemisorbed reactants and the release of products from the catalyst surface, we employed a VA-TPD experiment on both SnO_2 and ZrO_2. Each catalyst was impregnated with liquid VA (see details in section 1.2). Then samples were introduced in the TPD apparatus and the desorption profiles were shown in figure 8, revealing distinct desorption patterns for the two catalysts. For ZrO_2, the signal corresponding to 5-nonanone (m/z = 57) appeared between 300 and 450 °C. This, along with the concomitant detection of CO_2 (m/z = 44) and the very low signal for VA (m/z = 60), indicates that VA readily undergoes ketonization on the ZrO_2 surface. In contrast, the 5-nonanone peak for SnO_2 was found at a higher temperature and in much lower intensity, as compared to ZrO_2. Additionally, VA (m/z = 60) desorption was clearly observed for SnO_2 at about 400°C and 600 °C. These observations could be another evidence for potential differences in the VA ketonization mechanism on SnO_2 versus ZrO_2. The lower lattice energy of SnO_2 could lead to the formation of stable valerate intermediates that require higher temperatures for decomposition, explaining the delayed 5-nonanone desorption and the presence of desorbed VA at high temperatures.

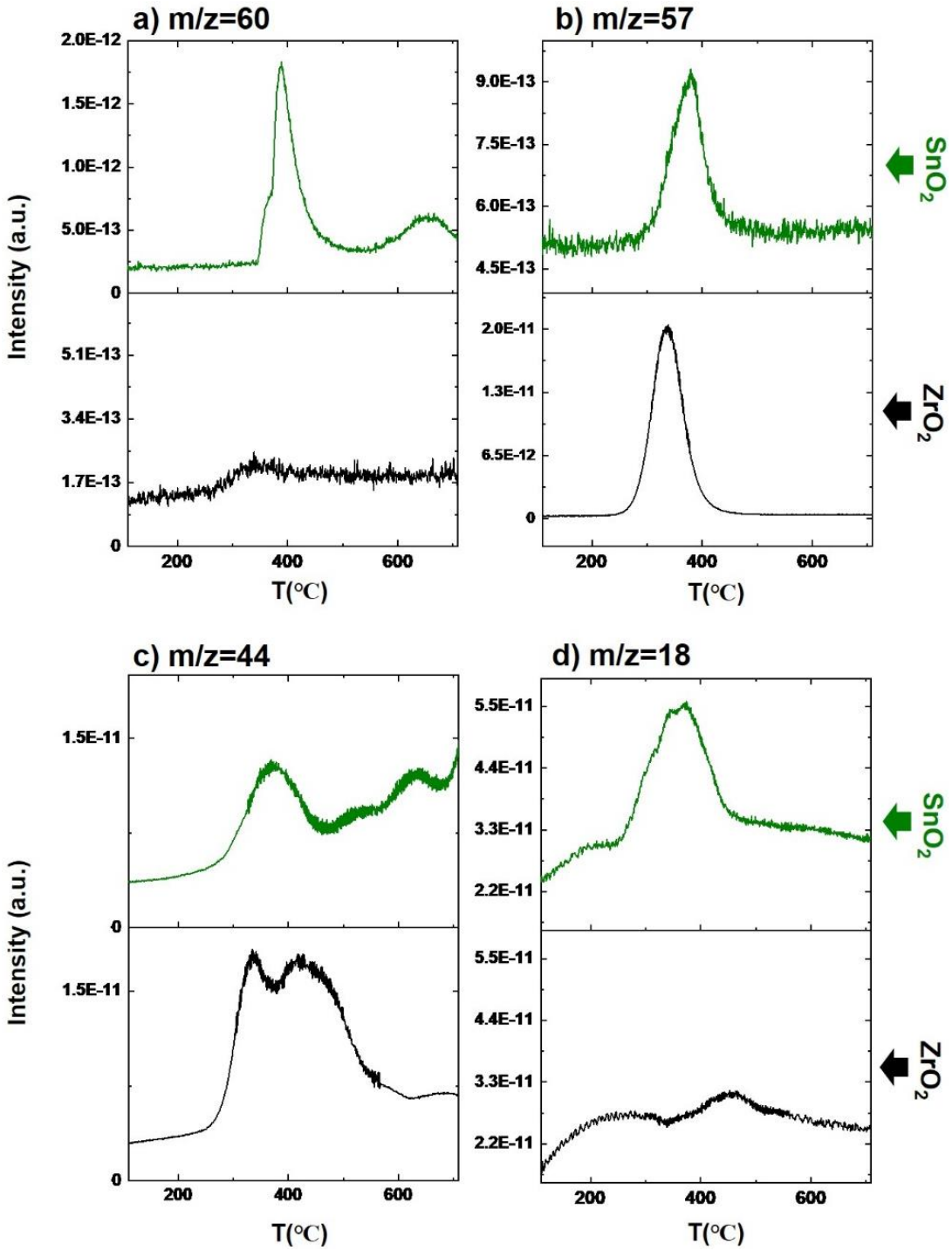

Figure 8. VA-TPD of SnO_2-VA and ZrO_2-VA catalysts. It has to be noted that the m/z 44 signal may also be attributed to fragmentation of VA in the MS, so that no conclusion can be drawn from CO_2 only.

2.4 Cr_2O_3: high lattice energy but no acido-basicity

To our knowledge, ketonization of VA over Cr_2O_3 has not been previously reported. Our initial investigation using commercially available Cr_2O_3 showed almost no catalytic activity though having high lattice energy. Primary characterization of the Cr_2O_3 revealed a neutral surface, lacking the requisite acidic and basic sites which were found to be crucial for ketonization reactions. However, Cr_2O_3 also possessed a very low surface area (2 m^2/g), hindering a definitive correlation between the lack of activity and the absence of acid-base sites. In order to address this limitation, we synthesized Cr_2O_3 using a peculiar sol-gel method method (SG, see details in ESI). We reasoned that this method would allow us to prepare a Cr_2O_3 sample with higher surface area, while maintaining the same crystal structure. XRD analysis (Figure 9) confirmed the successful synthesis of Cr_2O_3 (SG) with the hexagonal crystal phase characterized at 2θ = 24, 34, 36, 39, 41, 44, 50, 54, 63, 65, 73, 76, and 79° (JCPDS: # 96-900-8085) [34]. Diffraction peaks were smaller and much broader, consistent with the formation of small crystallites. This new sample had a SSA as high as 71 m^2/g and a pore volume of 0.40 cm^3/g.

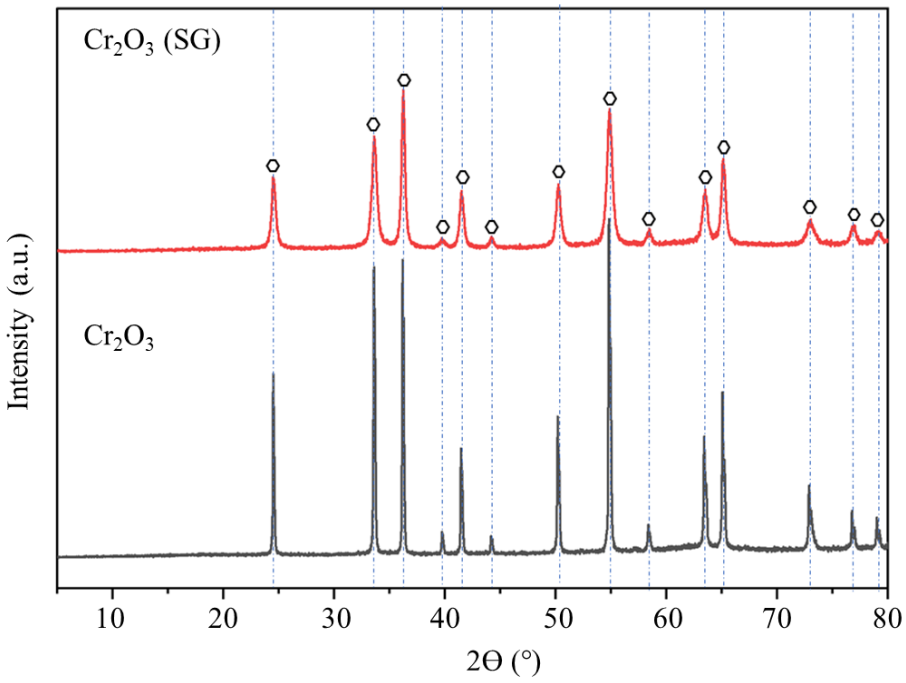

Figure 9. XRD Pattern of Cr_2O_3 and (TSG) Catalysts

Despite its increased surface area, Cr_2O_3 (SG) still exhibited extremely low concentration of acid and base sites, according to NH_3-TPD and CO_2-TPD analyses (Figure 10). In the ketonization of VA, Cr_2O_3 (SG) remained almost inactive. These combined findings confirm that, regardless of the high lattice energy of Cr_2O_3, surface acid-base sites are needed in the ketonization of valeric acid.

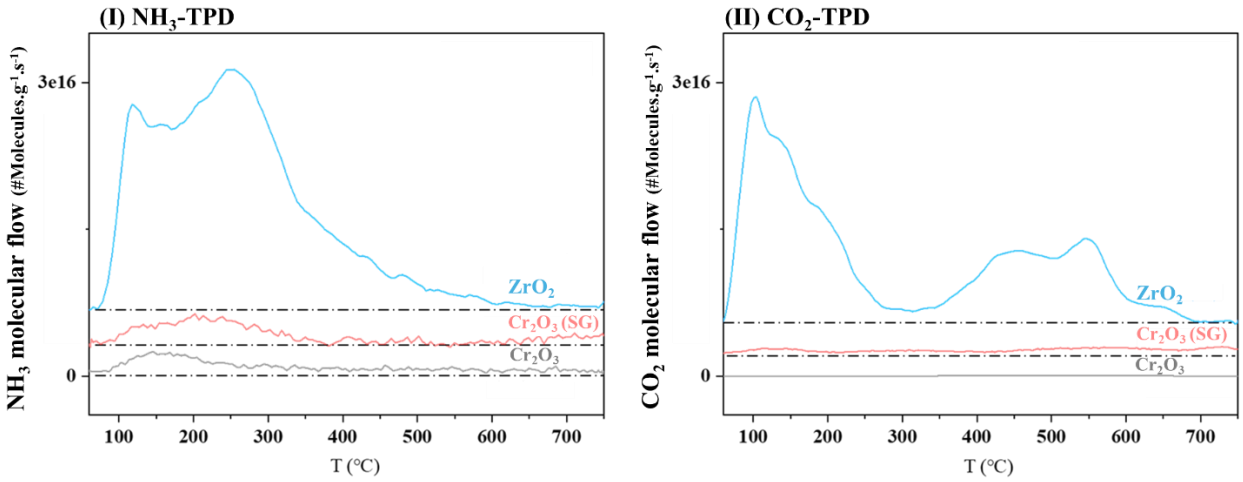

Figure 10. (I) NH_3-TPD and (II) CO_2-TPD Profiles of Cr_2O_3, and (SG) Catalysts

3 Conclusions

This study investigated the ketonization of VA over a series of metal oxide catalysts with varying lattice energies and acid-base properties. ZrO_2 and TiO_2 emerged as the most effective catalysts, exhibiting high conversion and selectivity towards 5-nonanone, a valuable biofuel precursor. This finding aligns with the generally observed trend that catalysts with high lattice energies demonstrate superior performance in the ketonization reaction. However, exceptions were encountered, such as Cr_2O_3 and Al_2O_3, which possess high lattice energy yet displayed minimal catalytic activity. This highlights the significance of both acid and base sites availability for efficient ketonization of VA. The investigation on the SnO_2, a catalyst with low lattice energy, provided additional insights. SnO_2 exhibited low catalytic activity compared to ZrO_2 at all temperatures studied. XRD analysis of used catalysts at low and high reaction

temperatures highlighted an alteration of the crystal structure of SnO_2, with formation of metallic Sn. Analysis of byproducts formed during SnO_2-catalyzed ketonization and TPD experiments for VA-impregnated catalysts showed the formation of short-chain carboxylic acids (not seen with good ketonization catalysts such as ZrO_2), arising from the cleavage of the α-carbon-hydrogen bond in valerate salts formed via the bulk mechanism. Overall, this study underscores the interplay between the lattice energy, acid-base character, and their synergy in governing ketonization efficiency. The findings contribute to a more comprehensive understanding of catalyst design principles for optimizing the conversion of biomass-derived carboxylic acids into valuable biofuel precursors.

Acknowledgements

This study was carried out within the framework of the ADV_BIO project financed by the SPF Economie (Service Public Federal Belgium) - Fonds de Transition Énergétique, call 2019−2020 subsidies.

Conflicts of interest

There are no conflicts of interest.

References

1. IEA, *World Energy Outlook 2022*. 2022, IEA, Paris, France.
2. Xu, H., et al., *Life Cycle Greenhouse Gas Emissions of Biodiesel and Renewable Diesel Production in the United States.* Environmental Science & Technology, 2022. **56**(12): p. 7512-7521.
3. Mujtaba, M., et al., *Lignocellulosic biomass from agricultural waste to the circular economy: a review with focus on biofuels, biocomposites and bioplastics.* Journal of Cleaner Production, 2023. **402**: p. 136815.
4. Alonzo, L.C.R., *Thermodynamic analysis of gasification and pyrolysis of lignocellulosic biomass: parametric study, energy/exergy balance and kinetic modelling*. 2020, Normandie Université.
5. Bennett, J.A., et al., *Acetic Acid Ketonization over Fe3O4/SiO2 for Pyrolysis Bio-Oil Upgrading.* 2017. **9**(9): p. 1648-1654.
6. Gholizadeh, M., X. Hu, and Q. Liu, *A mini review of the specialties of the bio-oils produced from pyrolysis of 20 different biomasses.* Renewable and Sustainable Energy Reviews, 2019. **114**: p. 109313.
7. Chen, H., *5 - Lignocellulose biorefinery product engineering*, in *Lignocellulose Biorefinery Engineering*, H. Chen, Editor. 2015, Woodhead Publishing. p. 125-165.
8. Gebresillase, M.N., et al., *Direct solvent-free selective hydrogenation of levulinic acid to valeric acid over multi-metal [NixCoyMnzAlw]-doped mesoporous silica catalysts.* Chemical Engineering Journal, 2023. **472**: p. 144591.
9. Goldberg, I. and J.S. Rokem, *Organic and Fatty Acid Production, Microbial*, in *Encyclopedia of Microbiology (Third Edition)*, M. Schaechter, Editor. 2009, Academic Press: Oxford. p. 421-442.
10. Adriaanse, N., H. Dekker, and J. Coops, *Heats of combustion of normal saturated fatty acids and their methyl esters.* Recueil des Travaux Chimiques des Pays-Bas, 1965. **84**(3): p. 393-407.
11. Martinez-Villarreal, S., et al., *Drop-in biofuels production from microalgae to hydrocarbons: Microalgal cultivation and harvesting, conversion pathways, economics and prospects for aviation.* Biomass and Bioenergy, 2022. **165**: p. 106555.
12. Serrano-Ruiz, J.C., D. Wang, and J.A. Dumesic, *Catalytic upgrading of levulinic acid to 5-nonanone.* Green Chemistry, 2010. **12**(4): p. 574-577.
13. Bond, J.Q., et al., *Integrated Catalytic Conversion of γ-Valerolactone to Liquid Alkenes for Transportation Fuels.* Science, 2010. **327**(5969): p. 1110-1114.
14. Friedel, C., *Ueber s. g. gemischte Acetone.* 1858. **108**(1): p. 122-125.
15. Pulido, A., et al., *Ketonic Decarboxylation Reaction Mechanism: A Combined Experimental and DFT Study.* 2013. **6**(1): p. 141-151.
16. Gliński, M., et al., *Catalytic ketonization over metal oxide catalysts. XIII. Comparative measurements of activity of oxides of 32 chemical elements in ketonization of propanoic acid.* Applied Catalysis A: General, 2014. **470**: p. 278-284.
17. Yamada, Y., et al., *Catalytic performance of rare earth oxides in ketonization of acetic acid.* Journal of Molecular Catalysis A: Chemical, 2011. **346**(1): p. 79-86.
18. Almutairi, S.T., E.F. Kozhevnikova, and I.V. Kozhevnikov, *Ketonisation of acetic acid on metal oxides: Catalyst activity, stability and mechanistic insights.* Applied Catalysis A: General, 2018. **565**: p. 135-145.
19. Ding, S., et al., *Ketonization of Propionic Acid to 3-Pentanone over CexZr1–xO2 Catalysts: The Importance of Acid–Base Balance.* Industrial & Engineering Chemistry Research, 2018. **57**(50): p. 17086-17096.

20. Kulyk, K., et al., *Kinetics of Valeric Acid Ketonization and Ketenization in Catalytic Pyrolysis on Nanosized SiO2, γ-Al2O3, CeO2/SiO2, Al2O3/SiO2 and TiO2/SiO2*. 2017. **18**(14): p. 1943-1955.
21. Panchenko, V.N., et al., *DRIFTS and UV–vis DRS study of valeric acid ketonization mechanism over ZrO2 in hydrogen atmosphere.* Journal of Molecular Catalysis A: Chemical, 2014. **388-389**: p. 133-140.
22. Zaytseva, Y.A., et al., *Effect of Gas Atmosphere on Catalytic Behaviour of Zirconia, Ceria and Ceria–Zirconia Catalysts in Valeric Acid Ketonization.* Topics in Catalysis, 2013. **56**(9): p. 846-855.
23. Gliński, M., J. Kijeński, and A.J.A.C.A.G. Jakubowski, *Ketones from monocarboxylic acids: Catalytic ketonization over oxide systems.* 1995. **128**(2): p. 209-217.
24. Boekaerts, B. and B.F. Sels, *Catalytic advancements in carboxylic acid ketonization and its perspectives on biomass valorisation.* Applied Catalysis B: Environmental, 2021. **283**: p. 119607.
25. Galsin, J.S., *Chapter 4 - Bonding in Solids*, in *Solid State Physics*, J.S. Galsin, Editor. 2019, Academic Press. p. 69-91.
26. Ladd, M.F.C. and W.H. Lee, *The calculation of lattice energies.* Journal of Inorganic and Nuclear Chemistry, 1959. **11**(4): p. 264-271.
27. Gliński, M. and J. Kijeński, *Catalytic Ketonization of Carboxylic Acids Synthesis of Saturated and Unsaturated Ketones.* Reaction Kinetics and Catalysis Letters, 2000. **69**(1): p. 123-128.
28. Pham, T.N., et al., *Ketonization of Carboxylic Acids: Mechanisms, Catalysts, and Implications for Biomass Conversion.* ACS Catalysis, 2013. **3**(11): p. 2456-2473.
29. Lu, F., et al., *Promotional effect of Ti doping on the ketonization of acetic acid over a CeO2 catalyst.* RSC Advances, 2017. **7**(36): p. 22017-22026.
30. Pestman, R., et al., *Reactions of Carboxylic Acids on Oxides: 2. Bimolecular Reaction of Aliphatic Acids to Ketones.* Journal of Catalysis, 1997. **168**(2): p. 265-272.
31. Snell, R.W. and B.H. Shanks, *Insights into the Ceria-Catalyzed Ketonization Reaction for Biofuels Applications.* ACS Catalysis, 2013. **3**(4): p. 783-789.
32. Degen, T., et al., *The HighScore suite.* Powder Diffraction, 2014. **29**(S2): p. S13-S18.
33. Shirasuka, K., et al., *The preparation of eta alumina and its structure.* 1976. **84**(976): p. 610-613.
34. McMurdie, H.F., et al., *Standard X-ray diffraction powder patterns from the JCPDS research associateship.* 1987. **2**(1): p. 41-52.
35. Bommer, H., *Die Gitterkonstanten der C-Formen der Oxyde der seltenen Erdmetalle.* Zeitschrift für anorganische und allgemeine Chemie, 1939. **241**(2-3): p. 273-280.
36. Wang, C., et al., *La2Co2Se2O3: A Quasi-Two-Dimensional Mott Insulator with Unusual Cobalt Spin State and Possible Orbital Ordering.* Journal of the American Chemical Society, 2010. **132**(20): p. 7069-7073.
37. Wyckoff, R.W.G. and R.W. Wyckoff, *Crystal structures*. Vol. 1. 1963: Interscience publishers New York.
38. Bumajdad, A., et al., *Controlled Synthesis of ZrO2 Nanoparticles with Tailored Size, Morphology and Crystal Phases via Organic/Inorganic Hybrid Films.* Scientific Reports, 2018. **8**(1): p. 3695.
39. Yashima, M. and S. Tsunekawa, *Structures and the oxygen deficiency of tetragonal and monoclinic zirconium oxide nanoparticles.* J Acta Crystallographica Section B: Structural Science, 2006. **62**(1): p. 161-164.

40. Zachariasen, W., *Untersuchungen über die Kristallstruktur von Sesquioxyden und Verbindungen ABO3.* %J Skrifter utgitt av det Norske Videnskaps-Akademi i Oslo, 1928. **1**: p. 1-165.
41. PEACOR, D.B., *High-temperature single-crystal study of the cristobalite inversion.* J Zeitschrift für Kristallographie-Crystalline Materials, 1973. **138**(1-6): p. 274-298.
42. Seki, H., et al., *High temperature structures of the rutile-type oxides, titanium dioxide and tin dioxide.* J Ceramic Association Japan, 1984. **92**: p. 219-223.
43. Yazdanpanah, M., et al., *The Underlying Catalytic Role of Oxygen Vacancies in Fatty Acid Methyl Esters Ketonization over TiOx Catalysts.* ChemSusChem, 2024. **17**(2): p. e202301033.
44. Kumar, R., et al., *Ketonization of oxygenated hydrocarbons on metal oxide based catalysts.* Catalysis Today, 2018. **302**: p. 16-49.
45. Yakerson, V.I., et al., *Catalytic ketonization of acetic acid over mixed catalysts ZrO2-Al2O3.* Bulletin of the Academy of Sciences of the USSR, Division of chemical science, 1966. **15**(1): p. 65-69.
46. Ignatchenko, A.V., *Multiscale approach for the optimization of ketones production from carboxylic acids by the decarboxylative ketonization reaction.* Catalysis Today, 2019. **338**: p. 3-17.
47. Ignatchenko, A.V., et al., *Ab initio study of the mechanism of carboxylic acids cross-ketonization on monoclinic zirconia via condensation to beta-keto acids followed by decarboxylation.* Molecular Catalysis, 2017. **441**: p. 35-62.
48. Pham, T.N., D. Shi, and D.E. Resasco, *Kinetics and Mechanism of Ketonization of Acetic Acid on Ru/TiO2 Catalyst.* Topics in Catalysis, 2014. **57**(6): p. 706-714.
49. Renz, M., *Ketonization of Carboxylic Acids by Decarboxylation: Mechanism and Scope.* 2005. **2005**(6): p. 979-988.